PUB in Quebec: A robust geomorphology-based deconvolution-reconvolution framework for the spatial transposition of hydrographs

Stéphane Ecrepont, Christophe Cudennec, F. Anctil, Anne Jaffrézic

PUB in Québec: A robust geomorphology-based deconvolution-reconvolution framework for the spatial transposition of hydrographs

Stéphane Ecrepont[1], Christophe Cudennec[1], François Anctil[2], Anne Jaffrézic[1]

[1]UMR SAS, AGROCAMPUS OUEST, INRA, 35000 Rennes, France

[2]Department of Civil and Water Engineering, Université Laval, Québec, QC, Canada

Correspondence to stephane.ecrepont@inra.fr

Highlights

- Successful geomorphology-based discharge prediction on snow influenced catchments.
- Model efficiency governed by both structural and circumstancial effects.
- Ghosh distance between catchments characterizes transposition configurations.
- Performances in pseudo-ungauged catchments open options for ungauged catchments.

Abstract

The flexibility and parsimony of transpositioning hydrographs using geomorphology-based deconvolution-reconvolution frameworks is particularly adapted to prediction in ungauged basins. Although already tested in semi-arid and oceanic-temperate hydro-climates, its predictions must be reproducible in a variety of hydrological contexts. The present study explores the nivo-pluvial hydrological regime using geomorphology-based hydrograph transposition between 21 gauged catchments ranging from 1.1 to 4466.4 km² in Québec, Canada, and constitutes a case study in prediction in ungauged basins. Three metrics were used to assess model performance for each donor-target pair: Nash Sutcliffe Efficiency (NSE), NSE calculated for the square root of discharge (NSE_{sqrt}), and Volumetric Efficiency. The classic transposition of hydrographs using the specific

discharge ratio, used as a reference, was almost always outperformed by the geomorphology-based approach. Good but seasonally variable performance values were obtained for several pairs of catchments, revealing simultaneous structural and situational effects. The difference in size, the physical distance between the gauged donor and its target ungauged catchment, and the season influenced the performance of the geomorphology-based transposition.

Keywords

Ungauged basin; Geomorphology; Hydrograph transposition; Scaling; Seasonality; Nivo-pluvial regime

1. Introduction

Prediction in Ungauged Basins (PUB), as an agenda-setting theme (Sivapalan et al., 2003), has triggered important methodological progress (Blöschl et al., 2013; Hrachowitz et al., 2013b) and practical advances (Pomeroy et al., 2013; Spence et al., 2013). Elementary and synthetic developments have been achieved, especially in terms of general understanding; similarity assessment and classification; and flexible hierarchical modelling approaches applied to annual and seasonal runoff, flow duration curves, low flows, and floods. Nevertheless, beyond the end of the International Association of Hydrological Sciences 2003-2012 decade on PUB, some methods remain to be explored, improved, or adapted to other hydrological settings. Key paths of further progress include comparative hydrology; transfer of knowledge from experimental catchments to data-scarce areas; and flexible approaches across contexts and scales, temporal variability, and densities of data availability (Blöschl et al., 2013; Hrachowitz et al., 2013a; Sivakumar, 2007). Runoff hydrographs remain particularly critical as they encompass the full temporal pattern of catchment hydrology and constitute the composite of all signatures and variabilities (McMillan et al., 2017; Parajka et al., 2013). In particular, robust simulation of discharge remains challenging at infra-daily time steps over

48 long periods for different sizes of catchments, due to event-level, seasonal, or interannual
49 hydrometeorological variability.

50 Within the general geomorphology-based unit hydrograph framework (Cudennec et al., 2004;
51 Franchini and O'Connell, 1996; Rigon et al., 2016; Rodríguez-Iturbe and Valdés, 1979), the family of
52 methods, which derives a transfer function from easily observable geomorphometric width and area
53 functions (Cudennec, 2007; Kirkby, 1976; Robinson et al., 1995; Snell and Sivapalan, 1994; Surkan,
54 1969), opens modelling opportunities which exploit an explicit structure, low calibration
55 requirements, and flexibility. For instance, Cudennec (2000) and Boudhraâ et al. (2006, 2009)
56 explored geomorphology-based transfer functions of water through the river network down to the
57 outlet of the catchment. Inversion of a transfer function deconvolutes the outlet discharge series into
58 a space-averaged net rainfall series, defined here as the hillslope response to a rainfall impulse, i.e.
59 the water flowing through the hillslope-river interface (Boudhraâ et al., 2018; Formetta et al., 2011;
60 Gupta and Mesa, 1988; Robinson and Sivapalan, 1996; Wang et al., 1981). The inversion has been
61 operationalized further (Menke, 1989; Tarantola, 1987; Tarantola and Valette, 1982) with verification
62 of the statistical distribution of errors, testing of several *a priori* options for initialization, and
63 sensitivity analysis of parameters (Boudhraâ et al., 2018; de Lavenne et al., 2015). Simulating the
64 discharge series at another outlet thus becomes possible by 1) assuming that the net rainfall series
65 can be spatially transferred or generalized from one or several (here one) gauged donor catchments
66 to an ungauged target catchment, based on nesting, neighbouring, or similarity configurations; 2)
67 estimating the geomorphology-based transfer function of the ungauged catchment, and 3)
68 convoluting these net rainfall series and the transfer function. Applications in the context of PUB
69 require robustness and parsimony of both the deconvolution and convolution steps. These qualities
70 are obtained by assuming linearity of the transfer functions used for the donor and target
71 catchments, which corresponds to an assumption and estimation of average flow velocity through
72 the river network of a given catchment, and the exclusion of hydraulic and geomorphological
73 dispersions. Fig. 1 summarises the two-step process.

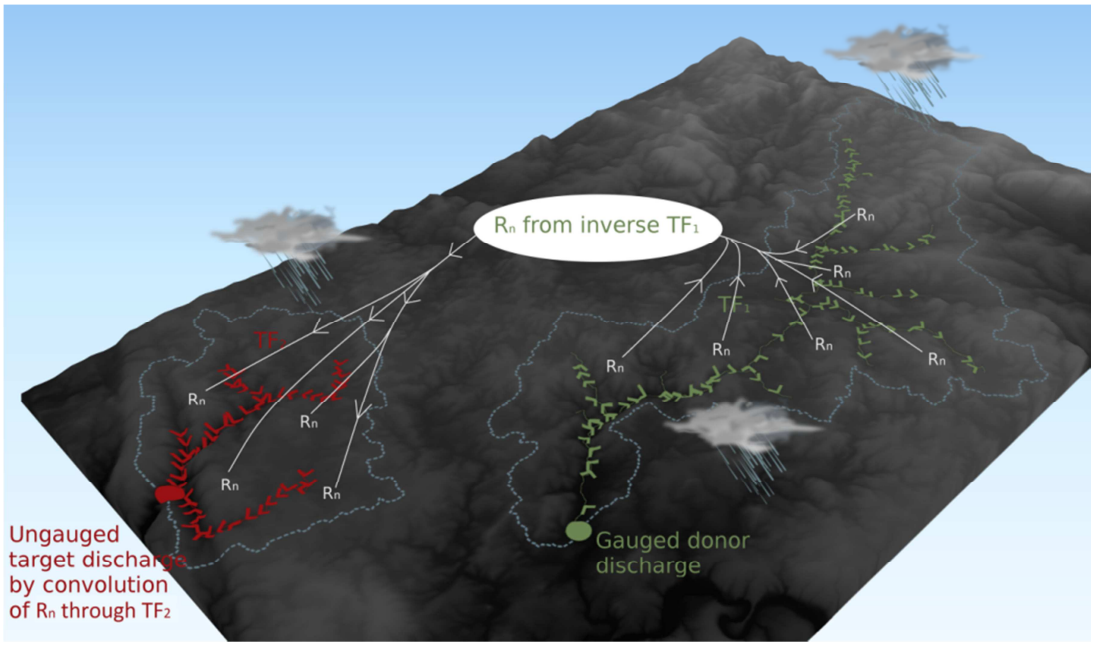

Figure 1. Diagram of geomorphology-based inversion-transposition of a hydrograph. The spatially-averaged net rainfall series (R_n) is estimated from deconvoluted discharge using the inversion of the transfer function (TF) of the gauged catchment (TF_1).It is then transposed to the ungauged catchment and convoluted using the ungauged TF (TF_2). Arrows indicate the direction of deconvolution (from downstream to upstream) and convolution (from upstream to downstream).

To date, this framework has been applied to two contrasting hydrological settings: semi-arid Tunisia and humid temperate France, relying on dense gauging networks and configurations, in which some gauged catchments were considered as pseudo-ungauged ones to provide blind references. The Horton-type rainfall-runoff dynamics of semi-arid Tunisia allowed for initial development of the framework due to the region's simple hillslope dynamics (Boudhraâ et al., 2018; Bull and Kirkby, 2002; Merheb et al., 2016) and simple characteristic time of events on small catchments up to several tens of km² in area (Nasri et al., 2004b). Yet the approach still faces challenges for larger catchments or areas (Chargui et al., 2013; Cudennec et al., (2005, 2016; Feki et al., 2012; Kingumbi et al., 2005), such as rainfall variability in space and time, and effects of infrastructure such as soil and water conservation installations and small dams (Lacombe et al., 2008; Nasri et al., 2004a; Ogilvie et al., 2016, 2018). A more systematic application in humid temperate Brittany, France, allowed further exploration of the articulation of hillslope-river network compartments, and hence the physical significance of the net rainfall signal and the strategy for pairing donor and target catchments or groups of catchments (de Lavenne et al., 2015), such as those of a coastal bay (de Lavenne and

Cudennec, 2014). Geomorphology-based transposition was also applied to the Loire River catchment (the largest one in France, ca. 110,000 km² at Mont-Jean-sur-Loire before tidal influence) and its related tributaries (de Lavenne et al., 2016). Using the mean net rainfall series estimated from the five closest catchments, results were generally of high quality according to several metrics. In addition, comparison to the top-kriging approach (Skøien et al., 2006) used as a reference showed that, on average, geomorphology-based transposition had similar and sometimes better results, which is promising given its methodological robustness and flexibility in using available data. These applications showed some adaptability to contrasting hydrological contexts and added values in modelling discharge series in (pseudo-) ungauged catchments, as well as limitations of the application domain.

The aim of this study was to apply and assess the relevance of geomorphology-based transposition in yet another hydrological context – Québec, Canada – which differs from previous regions in its hydrological regime, snow influence, physical geography, and gauging configurations. Data from national and academic hydrometric facilities allowed a variety of topological and geometric configurations to be explored. The data set was also excellent for exploring hydrographic and synoptic effects with a clear and homogeneous underlying geography. Hourly simulations were assessed using several metrics, and specific discharge was used as reference for comparison.

2. Materials and methods

2.1. Study area

The northern side of the Saint Lawrence River near Québec City has developed into a geologic interface between the Canadian Shield, composed of hard rocks (mafic-felsic-paragneiss), and the sedimentary Saint Lawrence valley, where carbonates and detrital rocks abound (Fig. 2). This geological setting underlies the land cover distribution, dominated by unmanaged forests and mountainous landscapes in the north and anthropogenic activities in the valley. In the study region, the mean interannual precipitation ranges from 1000 mm to the north, east, and west to 1400 mm in

the centre. Due to the topographic configuration and the presence of Gulf of Saint Lawrence and the Atlantic Ocean to the east, the Montmorency forest, north of Québec City, constitutes a 'hotspot' of precipitation, despite being relatively homogeneous (Fig. 2).

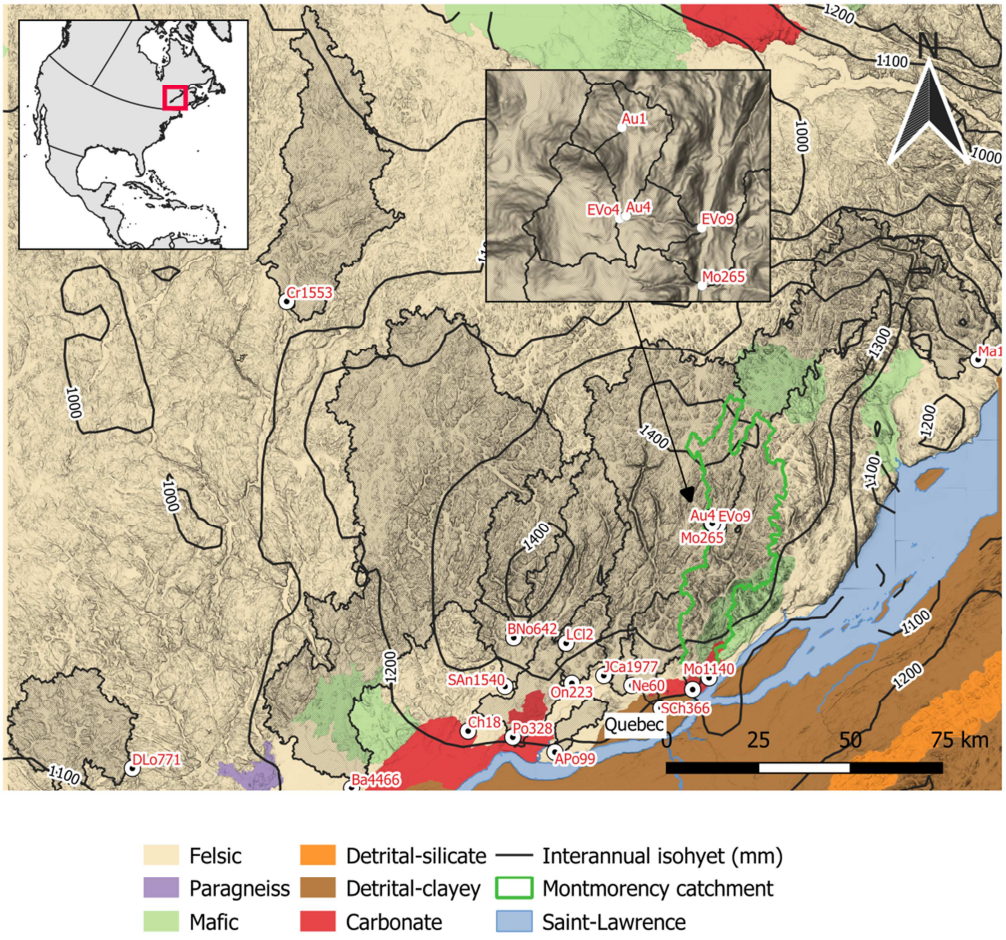

Figure 2. Geological map (MDDELCC and DEB, 2018) of the interface between the Canadian Shield and Saint Lawrence platform, splitting the region into a hard rock area to the north and a sedimentary area to the south. The 21 catchments used in the study are plotted at their outlets (see Table 1 for catchment names). Numbers in catchment codes represent surface areas (km^2).

The region is monitored with a configuration of gauging stations on 21 catchments, offering a long-term regional synoptic view of tributaries that flow mostly north-south, and including six nested catchments ranging from 1-1140 km² in the Montmorency River catchment (Tremblay et al., 2008) (Table 1). Codes are composed of initial letters of the full names and surface areas (km²). Most of the catchments are dominated by forests, except for Beauport (Be23), Nelson (Ne60), Aux Pommes

(Apo99), and Saint-Charles (SCh366), which are strongly artificial. The Des Aulnaies catchments (Au1 and Au4) also have a larger percentage of forest.

Table 1. Characteristics of studied catchments in order of increasing surface area. Bold codes identify nested catchments in the Montmorency River catchment (Au1, Au4, EVo4, EVo9, Mo265, Mo1140) and the two immediate neighbours (JCa1977, SCh366). Land cover data were provided by the MDDELCC and DEB (2018).

Name	Code	Area (km²)	Mean elevation (m)	Agriculture (%)	Unmanaged forest (%)	Managed forest (%)	Wetland (%)	Water (%)	Artificial (%)
Des Aulnaies	**Au1**	1.1	859.4	0	37.6	62.4	0	0	0
Décharge du lac Clair	LCl2	1.9	303.1	0	79.0	0	0	21.0	0
Des Aulnaies	**Au4**	3.5	818.9	0.3	70.2	24.7	3.6	0	1.3
Des Eaux Volées	**EVo4**	3.7	813.2	0	82.2	15.9	1.7	0	0.2
Des Eaux Volées	**EVo9**	9.0	798.3	0.1	80.5	16.4	2.5	0	0.5
La Chevrotière	Ch18	17.6	119.7	11.8	70.8	5.2	10.2	0.2	1.8
Beauport	Be23	22.6	145.7	5.7	31.6	0.4	0.2	0.3	61.8
Nelson	Ne60	60.1	218.7	7.1	69.7	2.0	4.0	0.6	16.6
Aux Pommes	APo99	98.6	137.3	29.1	51.4	1.1	7.7	0.3	10.5
Ontaritzi	On223	223.0	318.0	3.5	80.9	2.4	3.3	7.6	2.4
Montmorency	**Mo265**	264.8	857.9	0.0	80.5	11.8	4.2	2.2	1.3
Portneuf	Po328	327.6	165.5	22.7	62.7	1.6	2.7	2.7	7.5
Saint-Charles	**SCh366**	366.4	306.3	2.6	72.3	1.2	2.2	2.8	18.9
Bras du Nord	BNo642	641.8	568.8	0.6	81.2	10.4	2.8	5.0	0.1
Du Loup	DLo771	771.3	426.3	0	83.0	3.3	4.3	9.2	0.1
Montmorency	**Mo1140**	1139.8	717.3	0.1	82.9	9.4	2.8	2.5	2.4
Saint-Anne	SAn1540	1540.1	553.6	1.7	81.9	8.2	3.0	4.5	0.8
Croche	Cr1553	1553.4	389.6	0.0	79.6	8.5	6.3	5.1	0.4
Malbaie	Ma1693	1692.8	679.5	0.5	79.9	11.1	2.5	4.8	1.0
Jacques-Cartier	**JCa1977**	1976.5	716.4	0.5	82.2	7.8	3.7	4.6	1.3
Batiscan	Ba4466	4466.4	383.3	4.1	78.8	4.5	3.8	7.5	1.2

The organization of the study area splits the data set into three parts, according to the rivers that flow into the Saint Lawrence River mostly from the west (Saint Lawrence near Trois-Rivières) or the east (Saint Lawrence at Québec City, Saint Lawrence at La Malbaie) (Fig. 3).

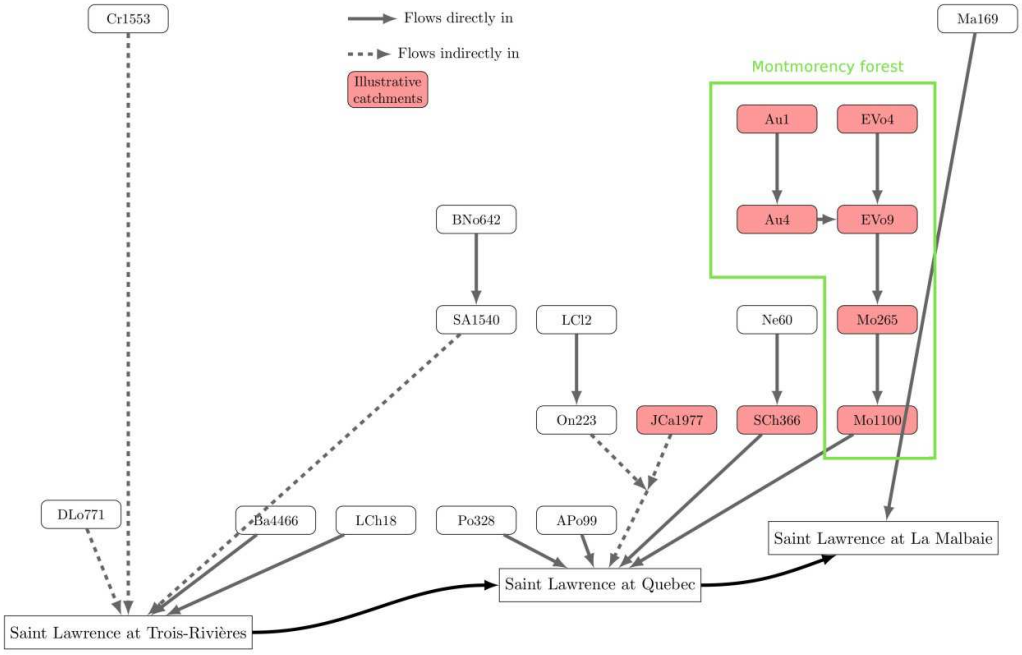

Figure 3. Topological diagram of the 21 catchments studied, according to their location on the study area and the order they flow into the Saint Lawrence. Catchments that are part of the Montmorency nesting configuration and its two immediate neighbours are highlighted in red. See Table 1 for catchment names. Numbers in catchment codes represent surface areas (km^2).

2.2. Data

Fifteen-minute streamflow data were obtained from a public web platform maintained by the Québec government (https://www.cehq.gouv.qc.ca/hydrometrie/historique_donnees/default.asp). Because of less frequent sampling before 2000, data from 1 April 2000 to 1 December 2016 were chosen. Quasi-continuous data are available after 2005, whereas some gaps appear before then. Winter observations are missing as they were influenced by ice. Geomorphological analysis was based on a 10 m-resolution DEM from the Québec government.

The study area has a humid continental climate. Its catchments are subject to a strong spring freshet and high autumnal flows, typical of a nivo-pluvial hydrological regime. Low flows occur in winter when snow accumulates on the ground and in summer when a dry spell develops during peak evapotranspiration. This contrasts with the French temperate context (de Lavenne et al., 2015,

158 2016), which has the same latitude as Québec, and even more with the Tunisian semi-arid context
159 (Boudhraâ et al., 2009, 2018).

160 ## 2.3. Methods

161 ### 2.3.1.Geomorphology-based transposition of discharge

162 Hydro-geomorphological analysis followed the approach of previous studies (Boudhraâ et al., 2009;
163 Boudhraâ et al., 2018; Cudennec, 2000; de Lavenne et al., 2015; de Lavenne et al., 2016). For each
164 catchment, water paths from a regular grid of points were identified through the hillslopes and the
165 river network (based on a threshold of 0.25 km²) down to the outlet, using GIS analysis (Aouissi et al.,
166 2013; Cudennec et al., 2004) based on GRASS 7.4.0 software. Thus the probability density function
167 (*pdf*) of the hydraulic length *L* (i.e. the length of the path through the river network to the outlet) was
168 assessed at the catchment level. The *pdf(L)* was then used to establish the transfer function *TF =*
169 *pdf(t)* through the river network based on average velocity $\bar{v}$. Use of an average velocity is consistent
170 with the classic simplifying and parsimonious assumption of linear transfer function through the river
171 network (Beven and Wood, 1993; Blöschl and Sivapalan, 1995; Franchini and O'Connell, 1996;
172 Grimaldi et al., 2012; Robinson and Sivapalan, 1996; Woods and Sivapalan, 1999). This assumption
173 remains especially acceptable for relatively small catchments (<500 km²), where hydrodynamic and
174 geomorphologic dispersions (unknown in ungauged catchments) can be ignored.

175 Discharge $Q(t)$ [m^3s^{-1}] at the catchment outlet can be simulated by convolution between the spatially-
176 averaged net rainfall series $R_n(t)$ [m] over the catchment and the transfer function TF, rescaled by
177 catchment surface area *S* [m²]:

178 $$Q(t) = S \int_0^t R_n(t-\tau) \cdot TF(\tau).d\tau \qquad (1)$$

179 This convolution can also be written as:

180 $$\boldsymbol{Q = TF \cdot R_n} \qquad (2)$$

where **Q** is the vector of discharge components (expressed in the same units as rainfall for convenience), **TF** the matrix composed of transfer function components, and $\mathbf{R_n}$ the net rainfall vector.

The net rainfall vector is estimated through inverse modelling (deconvolution) of observed discharges $\mathbf{Q_m}$, in accordance with the model defined by Eq. 2. A solution was found by minimizing the following expression (Boudhraâ et al., 2018; Cudennec, 2000; Menke, 1989):

$$\Phi(\boldsymbol{Q}, \boldsymbol{R_n}) = (\boldsymbol{Q} - \boldsymbol{Q_m})^t \boldsymbol{C_Q}^{-1} (\boldsymbol{Q} - \boldsymbol{Q_m})^t + \left(\boldsymbol{R_n} - \boldsymbol{R_n}^{apriori}\right)^t \boldsymbol{C_R}^{-1} (\boldsymbol{R_n} - \boldsymbol{R_n}^{apriori}) \quad (3)$$

where Φ is the likelihood function; $\mathbf{C_Q}$ and $\mathbf{C_R}$ covariance matrices of discharge and net rainfall, respectively (given by Eq. 5 and 6); $\mathbf{R_n}^{apriori}$ the vector of *a priori* net rainfall components; and t the symbol of a transposed matrix. Statistical distributions of both ($\mathbf{Q}$-$\mathbf{Q_m}$) and ($\mathbf{R_n}$-$\mathbf{R_n}^{aprio}$) were assumed to be normal and unbiased. Eq. 2 being a linear model, the solution satisfied:

$$\boldsymbol{R_n} = \boldsymbol{R_n}^{apriori} + \boldsymbol{C_R} \boldsymbol{TF}^t (\boldsymbol{TF}^t \boldsymbol{C_R} \boldsymbol{TF} + \boldsymbol{C_Q})^{-1} \boldsymbol{Q_m} - \boldsymbol{TF} \boldsymbol{R_n}^{apriori} \quad (4)$$

Menke (1989) described the stability, convergence, and uniqueness of the solution of such nonlinear problems in generic terms, and the geomorphology-based linear transfer function has been specifically assessed (Boudhraâ et al., 2009; Boudhraâ et al., 2018; Cudennec, 2000).

Eq. 3 and 4 introduce a *priori* information, formed by vector $\mathbf{R_n}^{apriori}$ and its associated covariance matrix $\mathbf{C_R}$, along with the level of confidence to be ascribed to this knowledge. According to Boudhraâ et al. (2018), who tested multiple options, the *a priori* net rainfall $\mathbf{R_n}^{apriori}$ to use is the specific discharge at the outlet of the catchment translated upstream along the time axis by the mean catchment lag time. The lag time is approximated from the mean hydraulic length divided by the characteristic velocity.

Observations suffer from measurement error, defined by the following covariance:

$$cov[Q_m(i), Q_m(j)] = \sigma_Q(i)\sigma_Q(j)exp\left[-\frac{1}{2}\left|\frac{(i-j)\Delta t}{T_Q}\right|^2\right] \quad (5)$$

where the standard deviation (SD) $\sigma_Q(i)$ of discharge measurement error is a linear function of discharge, according to parameters A_Q and B_Q: $\sigma_Q(i) = A_Q.Q_m(i) + B_Q$. The covariance expression is consistent with the hypothesis of a normal distribution, and T_Q stands for the decorrelation time of discharge errors.

Uncertainties in net rainfall are also estimated by $\mathbf{C_R}$,the covariance matrix of errors between *a priori* net rainfall $\mathbf{R_n^{apriori}}$ and true (unknown) net rainfall. The covariance is assumed to follow an exponential model:

$$cov[R_n(i), R_n(j)] = \sigma_R(i)\sigma_R(j)exp\left[-\frac{1}{2}\left|\frac{(i-j)\Delta t}{T_R}\right|^2\right] \quad (6)$$

where the SD $\sigma_R(i)$ of net rainfall error is a linear function of net rainfall, according to parameters A_R and B_R: $\sigma_R(i) = A_R.R_n(i) + B_R$. The covariance expression is consistent with the hypothesis of a normal distribution, and T_R stands for the decorrelation time of residuals between the *a priori* and true net hyetographs.

In this study, we used robust and versatile parameter values identified from a systematic sensitivity analysis(Boudhraâ et al., 2018; de Lavenne et al., 2015; de Lavenne et al., 2016) which equal 0.9, 0.15, 0.001, 0.01, 20 (min), and 1 (min) for A_R, A_Q, B_R, B_Q, T_R, and T_Q, respectively.

2.3.2. Velocity

The velocity of water flow through the river network was calculated for each rainfall event recorded. To prepare the data for PUB, velocity was regionalized based on all flood events in the data set (21 catchments from 2000-2016), following de Lavenne (2013), with slight adjustments in parameterization for consistency with the data set and its hydrological context. An event was detected if the slope of the rising limb of the hydrograph exceeded 0.25% h^{-1} and if the volume of water displaced during the event exceeded 0.01 mm. For every event detected, the rising time was

226 extracted, which allowed calculation of event mean velocity vs. the mean hydraulic length $\bar{L}$ of the
227 catchment. The distribution of velocities across seasons for the 21 catchments was ultimately
228 analysed to estimate regional velocity.

229 2.3.3. Systematic approach

230 Although the main purpose of geomorphology-based hydrological modelling is to simulate discharge
231 at the outlet of ungauged catchments, the present study explores a pseudo-ungauged approach to
232 allow comparison with observations (Fig. 2). To simulate a target pseudo-ungauged catchment from
233 a donor gauged catchment, a systematic approach was used involving all 21 gauged catchments. For
234 spring, summer, and autumn seasons, and the 2000-2016 period, each of the catchments was used
235 as the donor to, and then as the target of, all other catchments. This approach yielded 420 donor-
236 target combinations. Unlike de Lavenne et al. (2016), who used the five closest donors to estimate a
237 mean net rainfall series, and knowing the lower size and density of the gauging network considered,
238 we chose to follow a one-to-one approach to investigate successful pairs.

239 To assess simulation quality, transposition of specific discharge was used as a reference (Eq. 7):

240 $$Q_t = Q_d \left(\frac{S_t}{S_d}\right) \qquad (7)$$

241 where Q_t is the simulated discharge in the target catchment and Q_d the source discharge in the donor
242 catchment. S_t and S_d are areas of the target and donor catchments, respectively.

243 It assumes a linear relationship between discharge and catchment area, and homogeneity of runoff
244 generation in the donor and target catchments (Archfield and Vogel, 2010; Gianfagna et al., 2015;
245 Karlsen et al., 2016). The geostatistical top-kriging approach (Skøien et al., 2006), used as a reference
246 by de Lavenne et al. (2016) in the Loire River catchment (110,000 km², 389 gauging stations), could
247 not be used as a reference in the present study because of the lower gauging density in Québec.

Geomorphology-based transposition was first applied to the Montmorency catchment, which contains 6 gauging stations that monitor nested catchments ranging from 1-1140 km². As a thorough test case, 2013 was examined in detail as it had marked discharge fluctuations.

2.3.4.Verification metrics

Three goodness-of-fit metrics were calculated. To assess goodness-of-fit from geomorphology-based and specific discharge transpositions consistently, metrics were calculated only when observed discharge (Q_{obs}) and simulated discharge (Q_{sim}) were available, although missing values were plotted on hydrographs. Values were missing in early spring and late autumn in particular, when gauging stations were closed, and during some summer low flows.

Nash-Sutcliffe Efficiency (NSE) (Nash and Sutcliffe, 1970), a common metric used to assess hydrological model performance, was calculated:

$$NSE = 1 - \frac{\Sigma(Q_{obs,i} - Q_{sim,i})^2}{\Sigma(Q_{obs,i} - \bar{Q}_{obs})^2} \quad (8)$$

NSE ranges from $]-\infty; 1]$, equalling 0 when the model is as accurate as the mean of the observed discharge and 1 when the model provides a perfect fit. The NSE emphasises high flows as it is based on the mean squared error, which makes it sensitive to large errors (Muleta, 2012). A variant of the NSE, calculated for the square root of discharge (NSE_{sqrt}), was also calculated as it provides a compromise between emphasis on high or low flows (Oudin et al., 2006; Seiller et al., 2017):

$$NSE_{sqrt} = 1 - \frac{\Sigma(\sqrt{Q_{obs,i}} - \sqrt{Q_{sim,i}})^2}{\Sigma(\sqrt{Q_{obs,i}} - \overline{\sqrt{Q}}_{obs})^2} \quad (9)$$

Volumetric Efficiency (VE) (Criss and Winston, 2008) was also calculated as it estimates the bias in volume:

$$VE = 1 - \frac{\Sigma|Q_{obs} - Q_{sim}|}{\Sigma Q_{obs}} \quad (10)$$

VE has as same range and interpretation as NSE and NSE_{sqrt}.

To qualify metrics values, four classes were chosen for each criterion: “very good” when >0.66, “good” when 0.33-0.66, “average” when 0-0.33 and “poor” when <0. The terms “functioning pairs” and “failing pairs” are also used to describe pairs of donor-target catchments with “very good” or “poor” values for all metrics, respectively.

To compare the overall quality of the geomorphology-based transposition among metrics and catchments, heatmaps (Guttman, 1950; Sneath, 1957) were constructed and reordered according to the Ghosh distance of each catchment from the most south-westerly catchment, Du Loup (DLo771).

2.3.5.Ghosh distance-based statistical analysis

The Ghosh distance (Ghosh, 1951), which estimates a distance between two spatially gridded polygons, was estimated using the ‘rtop’ package (Skøien et al., 2014) of the R environment (R Development Core Team, 2017) for the 420 donor-target combinations. It was used to quantify the geometry of the 6 nested catchments and their neighbours to further analyse the quality of transpositions. A continuous and integrative method called “integrative function” was developed to assess model performance according to the Ghosh distance. Assuming a vector of metric $\boldsymbol{C}$ values $\boldsymbol{C} = (C_1, \dots, C_i, \dots, C_n)$ ordered by increasing Ghosh distance, the following function f was applied to each i^{th} position:

$$f_{int}(i) = f(\boldsymbol{C}(C_1, C_2, \dots, C_i)) \quad (12)$$

where f is the mean or the SD. The purpose of this integrative function is to assess the overall trend of metrics as Ghosh distance increases.

Ghosh distance was used to compare seasonal differences in hydrological behaviour.

290 3. Results

291 Results are organized into five sections: 1) regionalization of the characteristic velocity, 2) analysis of
292 hydrograph transpositions comparing geomorphology-based transposition and specific discharge, 3)
293 overall comparison of both approaches, 4) identification of heterogeneous behaviours for the entire
294 catchment data set, and 5) seasonal behaviours and physical significance of net rainfall based on the
295 Ghosh distance.

296 3.1. Regionalization of river flow velocity

297 A total of 19,894 rainfall-runoff events were identified from 1 April 2000 to 1 December 2016. A non-
298 linear relationship between characteristic velocity and mean hydraulic length existed which was
299 represented well with power-law regressions with similar coefficients (Fig. 4). Root mean squared
300 errors equalled 0.320, 0.302, and 0.419m.s^{-1} for spring, summer, and autumn, respectively. Median
301 velocities ranged from 0.005-2.392 m.s^{-1}. At the event scale, stream velocity varied by a factor of 2.2
302 to 5.8 from the 10th to 90th quantiles, respectively, depending on the catchment. Velocity remained
303 remarkably stable for each catchment around the median and across the three seasons (Fig. 4).

304

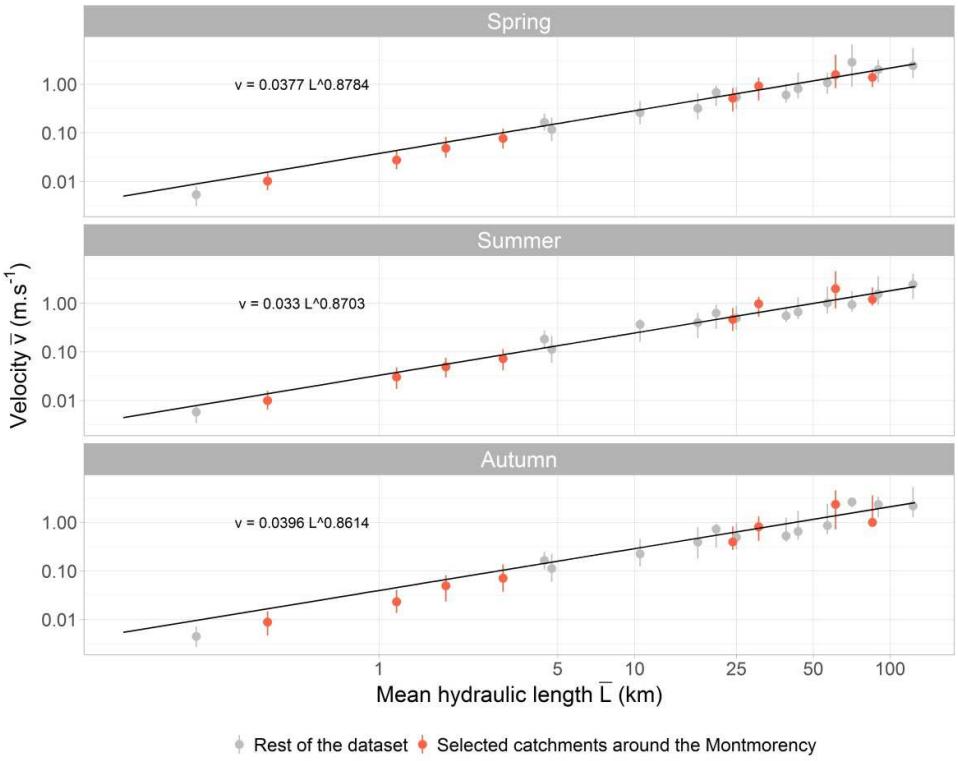

Figure 4. Velocity estimated by extracting the hydraulic length and rising time from 19,894 rainfall-runoff events in spring, summer, and autumn. Point range plots describe inter-event variability for each catchment; error bars represent 10th and 90th quantiles, while points are medians. Power law regression is drawn for each season, where $\bar{v}$ is the median velocity (m.s^{-1}) across the river network of the catchment considered and $\bar{L}$ the mean hydraulic length (km).

3.2. Comparison of hydrographs obtained from geomorphology-based (Q_g) and specific-discharge (Q_s) transposition

3.2.1.Montmorency catchment

When examining small neighbouring catchments Des Aulnaies (Au4) and Des Eaux Volées (EVo4), transposition was worse depending on the season and was sometimes “average” or “poor”, despite their proximity and similar size (Fig. 5). Geomorphology-based and specific-discharge transposition yielded similar results. Both approaches resulted in higher NSE and NSE_{sqrt} in the direction EVo4→Au4 than Au4→EVo4. VE was similar and “very good” in both directions, but the other metrics, especially NSE, were “average” or “poor” for Au4→EVo4. A seasonal pattern appeared with an underestimation of discharge in spring and late autumn (snowmelt and wet seasons) in the direction EVo4→Au4 but overestimation in summer and early autumn (dry season). When switching donor and target catchments, the inverse occurred. These two 4 km² catchments are nested within EVo9, Mo265 and Mo1140. The opposite bias observed between EVo4 and Au4 can be combined to

yield more accurate predictions.

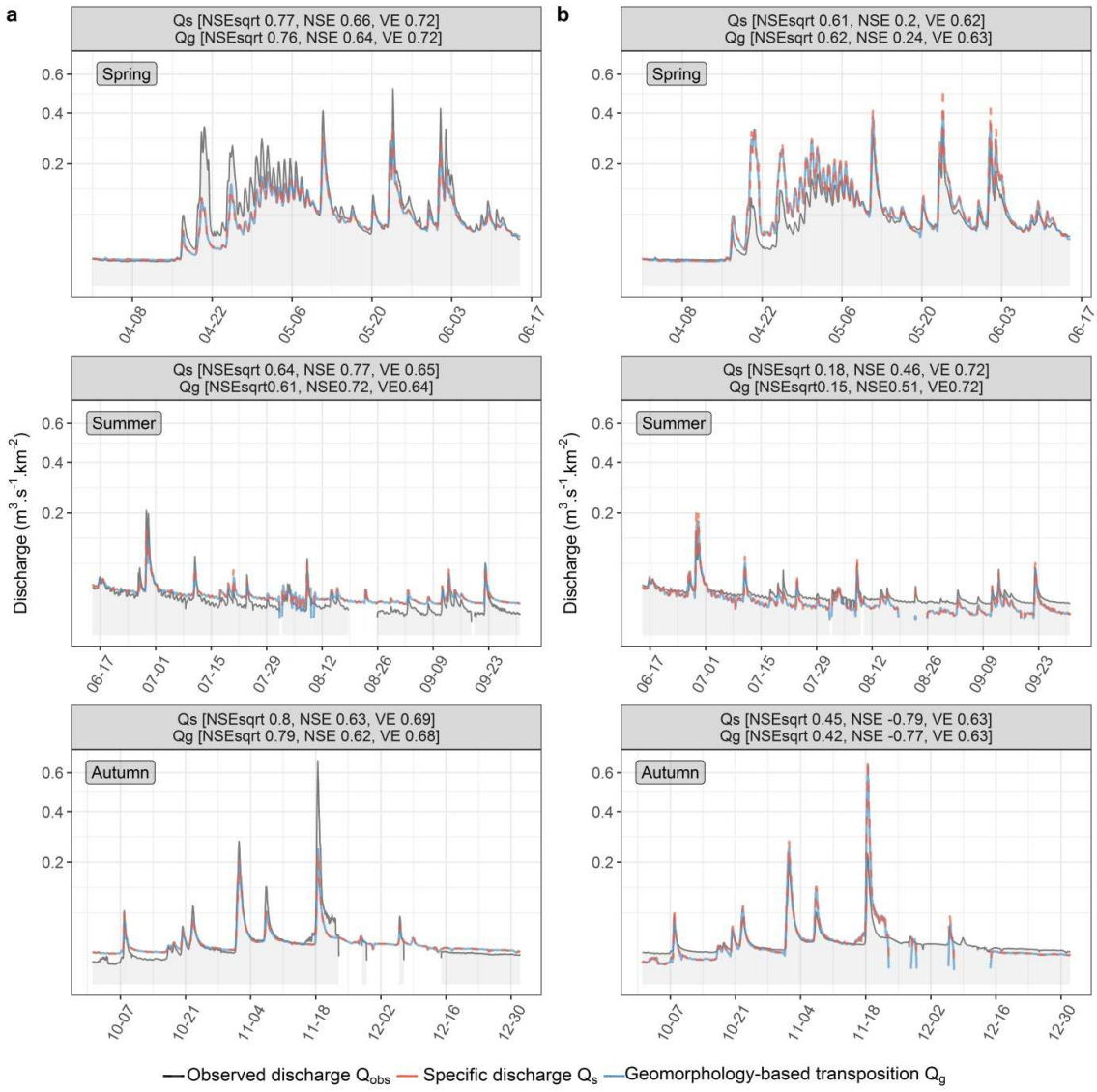

Figure 5. Observed discharge vs. discharge simulated by geomorphology-based transposition (Q_g) or specific-discharge transposition (Q_s) of two small neighbours from the Montmorency catchments: (a) EVo4→Au4 and (b) Au4→EVo4 in 2013 and their goodness-of-fit metrics – Nash Sutcliffe Efficiency (NSE), NSE calculated for the square root of discharge (NSE_{sqrt}), and Volumetric Efficiency (VE) – in spring, summer, and autumn.

Within the Montmorency catchment, both heterogeneous catchments Au1 and EVo4 were transposed to downstream nested catchments (summarized in Figure 6). Regardless of season and the metric, as target size increased, specific-discharge transposition increasingly failed. Conversely, for geomorphology-based transposition, although the same decrease was visible in summer, transposition quality remained stable (autumn) or increased at first and then decreased (spring).

Transposition quality towards Au4 and EVo9 was similar for both methods, for which geomorphology-based transposition largely outperformed specific-discharge transposition. In addition, specific-discharge transposition from Au1 was always worse than that from Evo4. For geomorphology-based transposition, Au1 was worse than Evo4 for small catchments, but this behaviour reversed as target catchment size increased.

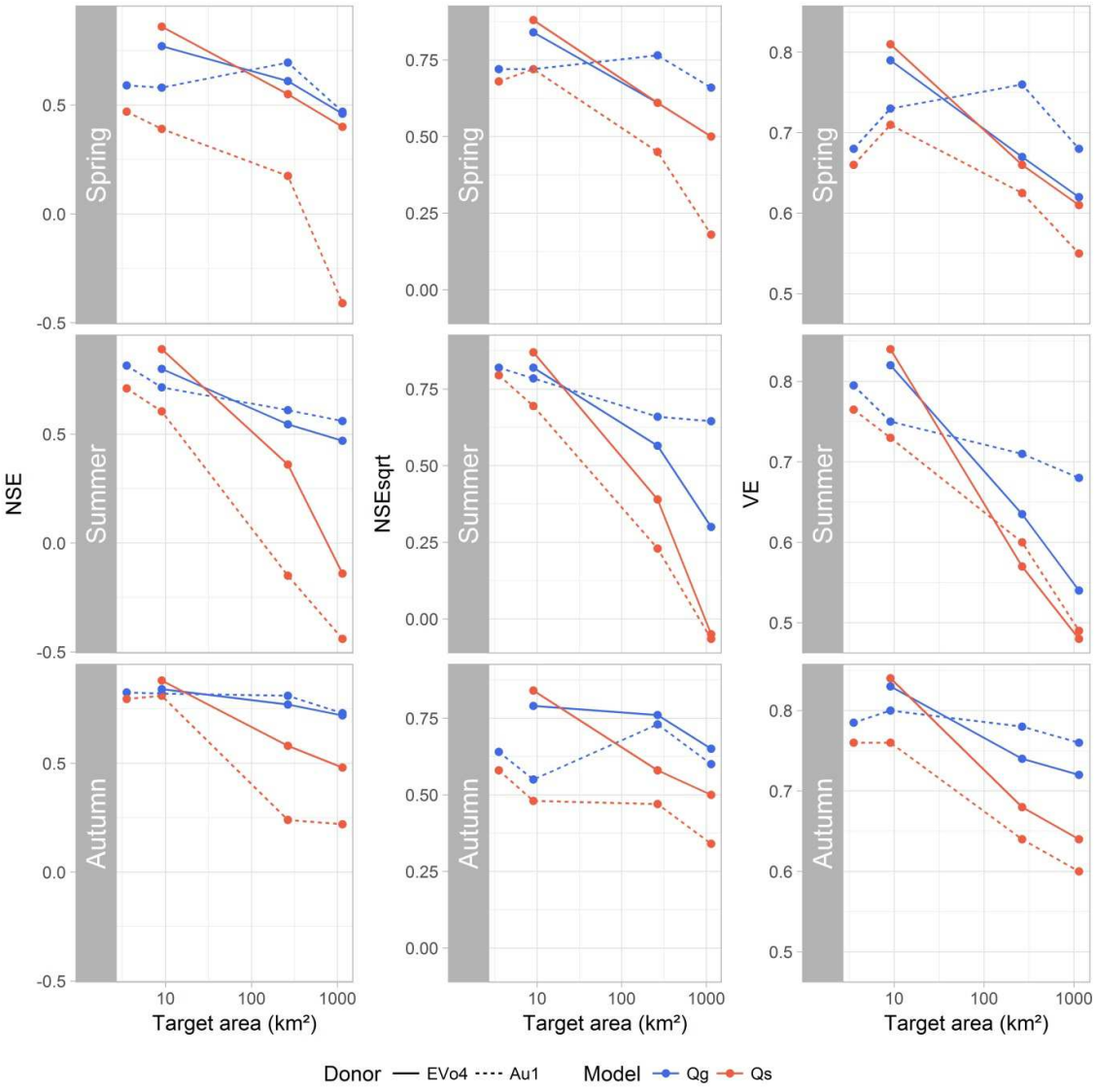

Figure 6. Geomorphology-based transposition (Q_g) and specific-discharge transposition (Q_s) metrics – Nash Sutcliffe Efficiency (NSE), NSE calculated for the square root of discharge (NSE_{sqrt}), and Volumetric Efficiency (VE) – from two small neighbouring catchments, Au1 and EVo4, to downstream nested catchments Au4, Evo9, Mo265, and M1140. Each point corresponds to the median of interannual seasonal simulations.

3.2.2. Between neighbouring catchments

Analysis then focused on the three largest neighbouring catchments studied (Mo1140, JCa1977, and SCh366). From Mo1140 to JCa1977, geomorphology-based transposition outperformed specific-discharge transposition according to all metrics (Fig. 7a). While the advantage was small according to VE ("very good" for all seasons), it was large for NSE and NSE_{sqrt} (0.41/0.11/0.81 vs. 0.13/-0.08/0.32 and 0.62/0.33/0.82 vs. 0.48/0.19/0.66 for spring, summer, and autumn, respectively). Specific-discharge transposition strongly overestimated observed discharge during freshet, while geomorphology-based transposition reproduced peak flow better. In addition, metrics differed greatly by season. Metrics of geomorphology-based transposition were "good" and "very good" in spring and autumn, respectively, but "average" for NSE and NSE_{sqrt} in summer. However, volume was well conserved, with "very good" VE values. The shape of the hydrograph was also reproduced well. From Mo1140 to SCh366, strong differences appeared in the hydrographs, especially seasonal behaviours (Fig. 7b). In 2013, Mo1140 discharged more intensively than SCh366, resulting in "poor" or "average" VE for each season. Despite synchronicity in the shape of their hydrographs, particularly visible for peak flows, volume was not simulated well. In addition, both geomorphology-based and specific-discharge transposition overestimated discharge during the first 20 days of May. In spring, Mo1140 flowed much more than SCh366, which must have been circumstancial (ie: depending on certain circumstances, especially the initial states), and did so for the rest of the year, which must

have been a structural difference.

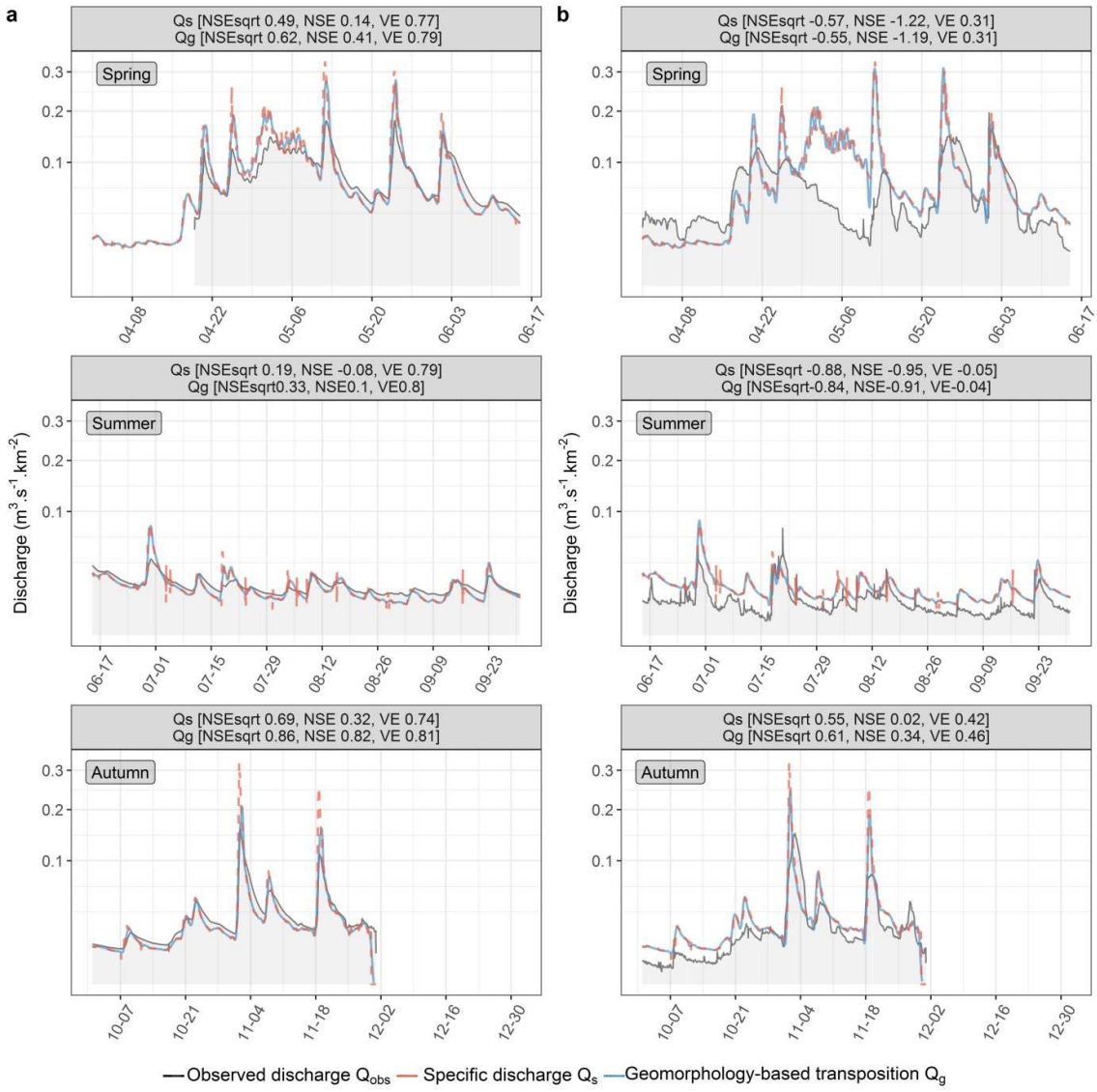

Figure 7. Observed discharge vs. discharge simulated by geomorphology-based transposition (Q_g) or specific-discharge transposition (Q_s) of (a) Mo1140 to JCa1977 and (b) Mo1140 to SCh366 in 2013 and their goodness-of-fit metrics – Nash Sutcliffe Efficiency (NSE), NSE calculated for the square root of discharge (NSE_{sqrt}), and Volumetric Efficiency (VE) – in spring, summer, and autumn.

3.3. Overall comparison of geomorphology-based transposed discharge (Q_g) and specific discharge (Q_s) hydrographs

A comparison of each metric for Q_g and Q_s as a function of the ratio of the surface area of the target catchment to that of the donor catchment shows similar results among metrics, but greater differences were observed for NSE (Fig. 8). Geomorphology-based transposition tended to yield

higher metric values than specific-discharge transposition, especially in the small→large direction (i.e. ratio > 1). In the large→small direction, results of the two approaches were more similar, although geomorphology-based transposition clearly had better results. Specific discharge transposition had the worst results in the large→small direction, but "poor" and erratic values were also obtained in the small→large direction. More similar results were observed for similarly sized donor and target catchments (ratio = 1). For NSE_{sqrt} and VE, a relationship in the form $y=x^2$ was observed, with a minimum at a surface area ratio close to 1.

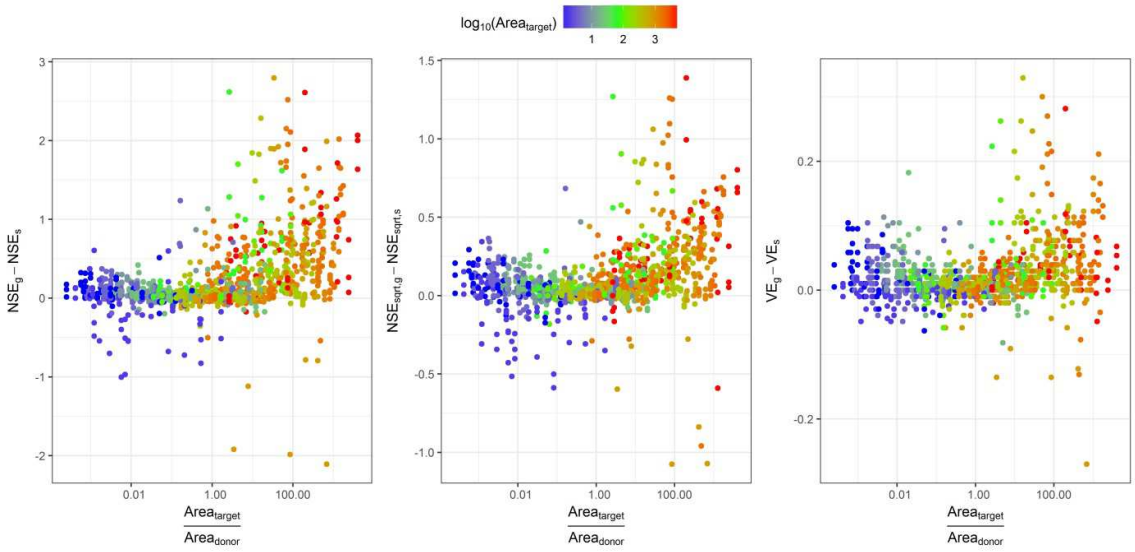

Figure 8. Differences in simulation metrics between geomorphology-based and specific-discharge transposition for all 420 configurations as a function of the ratio of the surface area of the target catchment to that of the donor catchment. On the x-axis, ratios greater than 1 identify simulations in the small→large direction . The y-axis is log-modulus transformed to constrain the wide range of positive and negative values (John and Draper, 1980).

3.4. Overview of geographic quality of geomorphology-based transposition through heatmaps

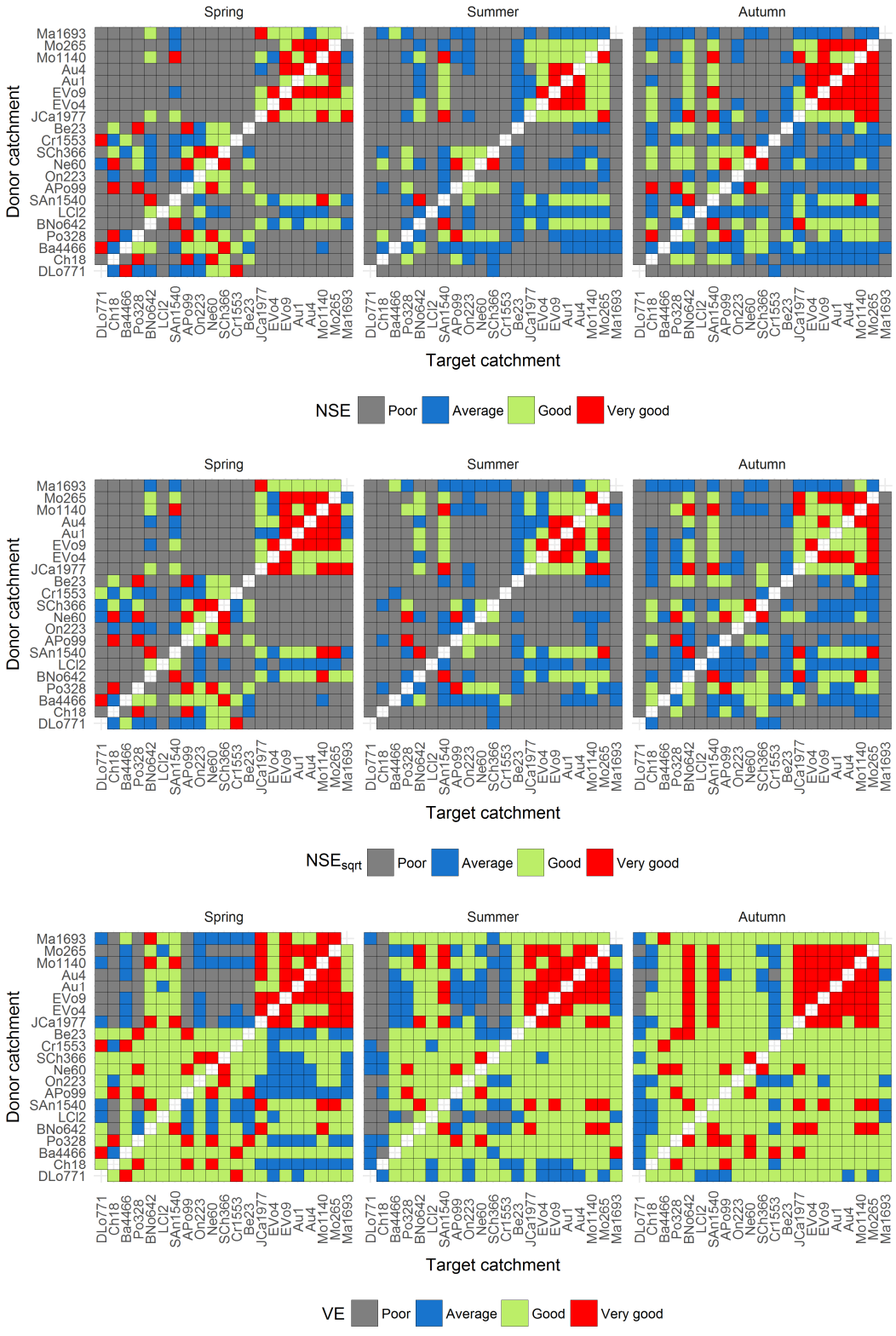

Figure 9. Heatmaps of Nash Sutcliffe Efficiency (NSE), NSE calculated for the square root of discharge (NSE$_{sqrt}$), and Volumetric Efficiency (VE) metrics for all 420 configurations of catchment transposition for all seasons and criteria. Catchments on each axis are ordered as a function of the Ghosh distance from the most south-westerly catchment,

DLo771. Metrics are "poor" when <0, "average" when 0-0.33, "good" when 0.33-0.66, and "very good" when >0.66. Numbers in catchment codes represent surface areas (km^2).

According to the heatmaps, NSE was a more challenging metric than NSE_{sqrt} and VE (Fig. 9). The volume of water (VE) was relatively homogeneous in the data set, unlike high flows (NSE). Most NSE_{sqrt} quality classes were identical to those of NSE. Overall, most of the catchments conserved a similar volume (VE), while the pattern of functioning/failing pairs remained nearly the same among metrics.

The geographic ordering of the heatmaps revealed pairs of properly functioning geomorphology-based transposition patterns that were consistent among metrics. The highest metrics were obtained between Montmorency catchments (EVo4-9, Au1-4, Mo265-1140, and JCa1977) and those to the west-north-west (BNo642, San1540 and LCl2, except Cr1553). Lower metrics were obtained between Montmorency catchments and the most distant ones (Ba4466, DLo771, Ch18, Po328). Other "poor" metrics were obtained between Montmorency catchments and coastal catchments along the Saint Lawrence River (APo99, On223, Ne60, SCh366, and Be23). In any case, metrics were generally higher when nearby catchments were transposed (Fig. 9).

Patterns of similarity were observed among seasons. Spring had the most "very good" metrics, followed by autumn and summer. Spring also had the most "poor" metrics, followed by summer and autumn. In autumn, metrics values were generally more homogeneous over the entire catchment.

3.5. Ghosh distance analysis

A double effect on Ghosh distances appeared for both small→large and large→small transposition directions, as the overall decrease was also affected by seasonality (Fig. 10). For all metrics and both directions, as Ghosh distance increased, the integrative mean decreased. While the rate of decrease was low up to a Ghosh distance of ca. 25 km, it increased substantially afterwards. The effect was greater for the integrative SD. As Ghosh distance increased, the variability/range of the integrative SD increased, but the pattern differed between directions. For large→small transposition, the integrative SD tended to increase at a higher rate at shorter distances (<25 km), while for

small→large transposition, the integrative SD increased continuously. More generally, autumn, as well as large→small transposition, had a more linear response.

None of the integrative mean metrics was “very good” at longer Ghosh distances; instead, they were restricted to a specific maximum value that decreased with Ghosh distance. Beyond ca. 100 km, the integrative mean of metrics rarely reached “good” or “average” values for small→large transposition. For large→small transposition, this threshold increased to ca. 150 km. Variability (via the integrative SD) also differed, revealing strong seasonal heterogeneities. For instance, in the small→large direction, integrative means were generally higher and decreased more slowly in autumn than in summer or spring. In the opposite direction, the spring integrative mean was higher than that in autumn, except for VE, and this trend reversed itself beyond 50 km. A similar pattern was observed for all metrics: while autumn was almost always better, summer outperformed spring, except from 20-50 km. In summer, and less so in autumn, the integrative SD was generally higher at short Ghosh distances (<25 km), then increased substantially. In spring, the integrative SD increased slowly up to 40 km before reaching the highest values among all seasons. This was particularly visible in the small→large direction. For both directions, the relationship between the integrative mean and Ghosh distance was similar among metrics, with stability until 20 km, followed by a decrease. For both directions, integrative mean VE was highest in autumn. This was also supported by the smaller increase in the integrative SD of VE. The integrative SD and mean of NSE curves each had similar shape in autumn and summer, especially in the large→small direction. More generally, the integrative SD increased more slowly in the large→small than small→large direction. In addition, the worst values in the large→small direction occurred for the smallest target catchments, especially for NSE and NSE_{sqrt}.

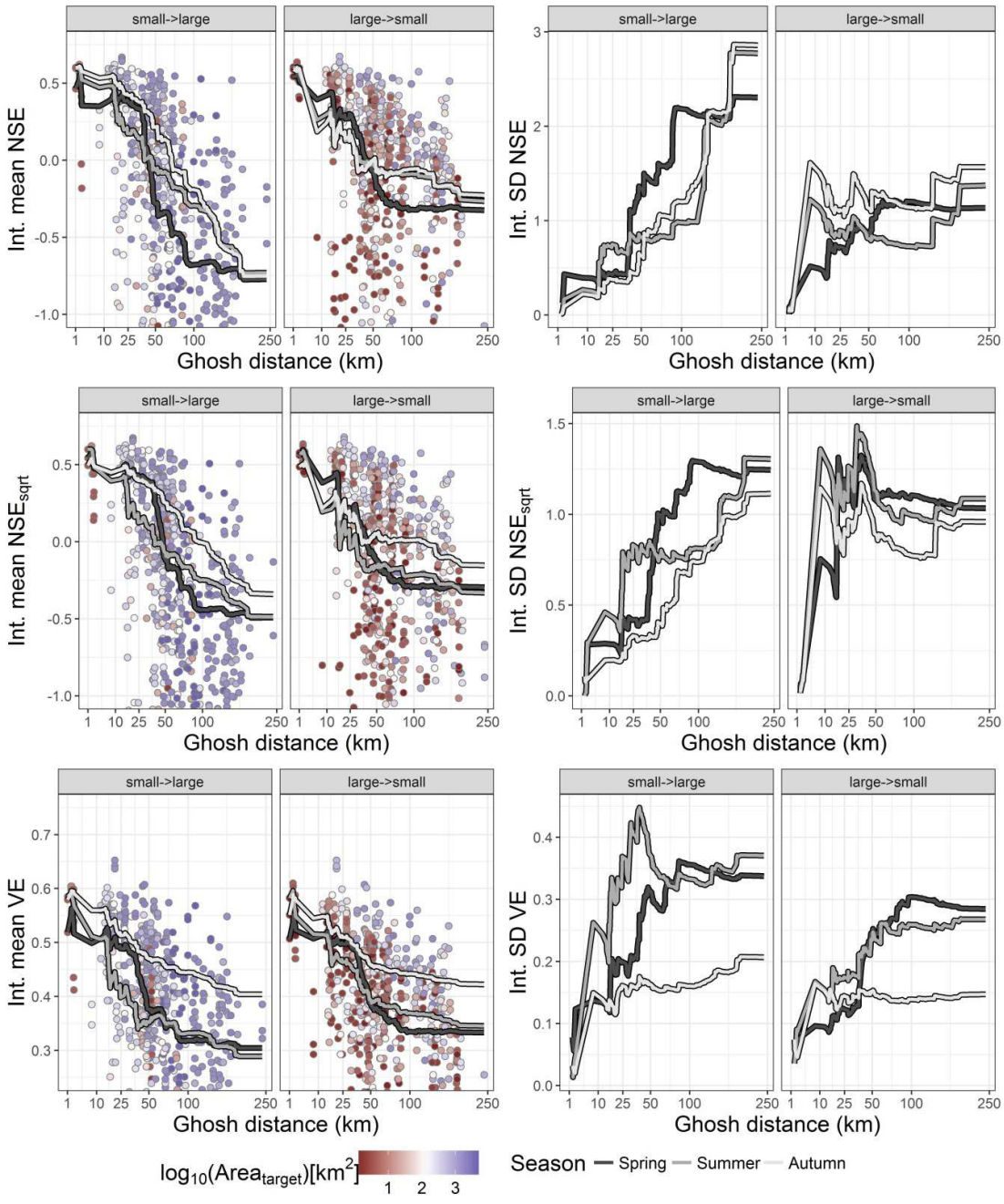

438

439 **Figure 10. Assessing geomorphology-based transposition as a function of donor-target distance (Ghosh), according to (a)**
440 **Nash-Sutcliffe Efficiency (NSE), (b) NSE of the square root of discharge (NSE$_{sqrt}$), and (c) Volumetric Efficiency (VE) for**
441 **spring, summer and autumn and by directions of transposition by catchment area. For each metric, the two left graphs**
442 **represent simulations from smaller to larger catchments (small→large), while the two right graphs represent the inverse**
443 **(large→small). The integrative mean axis is log-modulus transformed (John and Draper, 1980).**

444

445 4. Discussion

446 4.1. Performance in a new hydrological context

447 Several findings emerge from these results, giving geomorphology-based transposition a net
448 advantage over specific-discharge transposition, used here as a reference method for spatial
449 transposition of hydrographs. Geomorphology-based transposition uses structural information of the
450 stream network to construct a realistic transfer function most likely to distribute net rainfall
451 accurately in time. As a major parameter of this approach, stream characteristic velocities were
452 stable across seasons in each catchment. River flow velocity depends essentially on the morphology
453 and physical properties of the stream network, which are structural. Stability is also consistent with
454 the intrinsic conceptualization of the geomorphology-based framework, including the articulation
455 between hillslopes and the river network. The velocity considered refers to water dynamics across a
456 river network; they are related to non-seasonal river hydraulics and not to water dynamics across the
457 hillslope, which are much more season- and event-dependent.
458 Simulations were evaluated using three metrics: NSE, NSE_{sqrt}, and VE. Overall, for 420 pairs and three
459 seasons, the 1260 simulations ranged from (first to third quartiles) -0.87 to 0.35, -0.89 to 0.34, and
460 0.32 to 0.6 for NSE, NSE_{sqrt}, and VE, respectively. In Tunisia, Boudhraâ et al. (2009) used four
461 neighbouring catchments (3.16-192 km^2) in a one-to-one approach. Based on two hydrological
462 events following a convective storm, NSE ranged from 0.82-0.99. The dominance of Hortonian runoff
463 led to excellent performance values. For six catchments in Brittany (4.9-316 km^2), also using a one-to-
464 one approach, de Lavenne (2013) obtained NSE of 0.01-0.90 at the annual scale. In another study, de
465 Lavenne et al. (2016)estimated mean net rainfall of the target catchment from the five closest Ghosh
466 donors and then convoluted. Evaluation at the interannual scale (>3 years simulated) yielded first
467 and third quartiles of NSE equal to 0.55 and 0.86, respectively.
468

469 4.2. Structural similarity

Hydrographs of Q_g and Q_s showed infra-seasonal heterogeneity depending on the pair of catchments studied. The first example of catchments Mo1140 and Mo265 illustrated classic nesting of two meso-scale catchments with apparent similarity in geography and hydroclimate. This is consistent with the "very good" results obtained for both Q_g and Q_s, despite non-negligible error in 2013 autumnal floods. Mo1140 aggregates many sub-catchments, such as EVo4 and Au4 that function differently despite proximity and similarities in geography and hydroclimate. Discharge inverted in spring and summer, with Au4 flowing strongly when snowmelt began, while EVo4 started flowing later. During summer, however, EVo4 flowed more strongly than Au4, suggesting a difference in hydrological behaviour or delayed snowmelt. This simple desynchronization may be smoothed by ensemble modelling of two spatially closed catchments with equal weights. There was a clear difference in runoff generation between EVo4 and Au4 despite their proximity and apparent similarity. Catchments Au1, Au4, and EVo4 have 38%, 70% and 82% of forested land, respectively, but also 62%, 25% and 16% of timberland, respectively (Table 1). Following the general assumption of a Representative Elementary Area of 1-15 km² (Blöschl et al., 1995; Fan and Bras, 1995; Wood et al., 1988), the heterogeneity of hillslope topography, geography, and hydrological conditions may question the representativeness of catchments such as Au1, Au4, and EVo4 even though they belong to an apparently homogeneous region. This observation is transposable to Mo1140: heterogeneous low-level behaviours resulted in different responses of the two nested catchments. Interestingly, there was a difference between specific-discharge and geomorphology-based transposition from Au1 and EVo4 to downstream catchments. Evo4 was initially more representative of downstream catchments but became less so as target size increased. This pattern reveals the structural evolution of the catchment and the associated hydrological signature from *a priori* similar hydrological sub-units.

Between neighbours, the lack of nested similarity between upstream-downstream hydrological responses rendered transposition more difficult. This was seen in transposed hydrographs for Mo1140 to JCa1977 and Mo1140 to SCh366, both of which had lower metric values and large

variations across seasons. However, JCa1977 and SCh366 clearly differed, the former flowing like Mo1140, while the later was not synchronized and showed substantial bias in water volume (via VE). JCa1977 was more similar to Mo1140 in many respects (Table 1). SCh366 lies more to the south and yet remains in the calcareous Saint Lawrence Plateau, unlike Mo1140, which drains the Grenvillien bedrock further to the north. The calcareous bedrock may modify groundwater-river exchange and increase infiltration, unlike the Grenvillien, which increases surface runoff. In addition, the Saint Charles River drains 18.9% of artificial area vs. 2.4% for the Montmorency River, which significantly modifies hydrological processes (Table 1). The large difference observed in spring may result from snowpack, which is deeper in the Montmorency catchment. This is a good example of a spatially close pair of catchments for which hydrograph transposition fails because of differences in the input (snowpack and rainfall quantity, and hence net rainfall) and/or geography.

4.3. Circumstancial component

Heatmaps were used to identify a structural effect (transposition pairs functioning or failing) and a supplementary circumstancial effect. The former was observed in the relative similarity of functioning and failing pairs among heatmaps; however, differences appeared among seasons. For instance, most transpositions between catchments DLo771, La Chevrotière (Ch18), and Croche (Cr1553) failed regardless of the season and metric because of structural dissimilarities. For instance, metric values were more homogeneous and transposition failed less in autumn. Volume was generally reproduced well (VE) due to spatially homogeneous climatic forcing. Water flow dynamics varied greatly (NSE and NSE_{sqrt}), due more to different dominant flow paths or net rainfall variability at the event scale. Spring is dominated by snowmelt on saturated or frozen soils. Production processes from hillslopes are more homogeneous and mainly physically oriented (no biological activities), despite distances between catchments, increasing conservation of water balance in early spring, but a decorrelation during the transition to summer. This was visible in the large number of both “very good” and “poor” metrics. Summer accentuates heterogeneous behaviours, but

transposition remains a valid option between geographically close catchments. Summer is dominated by low flows without many hydrological peaks; performance is thus determined mostly by base flow discharges. During this period, metrics were more homogeneous than in spring, but only a few were "very good". In autumn, following rewetting of soils and longer hydrological events, metric values were generally higher, implying a tendency to return to spatial homogeneity.

4.4. Evidence of structural and circumstancial similarities through Ghosh distance analysis

Hydrograph transposition between a pair of catchments functions when both experience a simultaneous net rainfall event. Transposition between north-eastern and south-western catchments failed because the longer distances decreased the physical significance of net rainfall between catchments. Transposition between northern catchments (Mo1140, Mo265, Au1, Au4, EVo4, EVo9, SAn1540, BNo642, and JCa1977) and southern ones flowing into the Saint Lawrence (APo99, On223, Ne60, SCh366, and Be23) also failed, as seen between Mo1140 and SCh366. These results reveal that the distance between the catchments to be transposed should be kept in mind. In this study, this distance effect was assessed using the Ghosh distance. The study area has a climatic gradient from catchments in the north-east (Montmorency) (higher precipitation and elevation, lower temperature) to those in the south-west (lower precipitation and elevation, higher temperature). Hydrograph transposition was influenced by this gradient, which increases with distance. Hydrology is driven by snowmelt and synoptic events in spring, by convective events in summer, and by synoptic events again in autumn. The flow signal resulting from these types of climatic forcing is derived directly from the net rainfall entering the stream network, which is the variable used for geomorphology-based transposition. During snowmelt, net rainfall is produced mainly by overland flow after an increase in net radiation and air temperature (Dunne and Black, 1971; Kane and Stein, 1983). Net radiation depends greatly on catchment morphology and orientation, resulting in heterogeneous behaviours at the daily scale. Conversely, air temperature can be the same over a large area, resulting in homogeneous snowmelt at the catchment scale, especially at similar latitudes.

546 Overall, assuming similar snowpack among catchments, net rainfall should follow the assumption of
547 spatial homogeneity more closely in spring, leading to better transposition of hydrographs and
548 volume conservation. However, for longer distances, differing snowpack and snowmelt rates lead to
549 heterogeneity in hydrograph transposition, as illustrated by Mo1140 to SCh366. During the transition
550 between spring and summer, heterogeneous metric values appeared, especially for longer distances,
551 because of different snowpack depths, as illustrated by large heterogeneities in heatmap zones. In
552 summer, hillslopes are disconnected from groundwater, the latter sustaining base flow in the stream.
553 Convective events such as storms are highly heterogeneous in space and time; consequently, soil
554 moisture and water levels in hydrological compartments (i.e. groundwater, hillslope, and riparian
555 areas) may differ greatly between catchments, producing different amounts of net rainfall at the
556 event scale. Because of the assumption of spatially homogeneous net rainfall, hydrograph
557 transposition may be more difficult in summer than in spring (with its freshet). However, this effect
558 has much less influence in Québec than in the Tunisian semi-arid context previously explored.
559 Indeed, Hortonian overflow is the dominant process involved in runoff in Tunisia; hence, net rainfall
560 time series there closely follow the space-time variability in rainfall, which can be high for convective
561 events. Dominant flow paths evolve according to hydrological conditions and rainfall intensity. In a
562 natural catchment and during intense rainfall, net rainfall is dominated more by the rainfall itself and
563 may be more homogeneous over short distances. It may also explain the strong decrease in metric
564 values in summer and the sudden increase in variability in VE beyond 40 km. Autumn is characterized
565 by inversion of the water balance and progressive rewetting and filling of hydrological
566 compartments, as well as synoptic events. As a consequence, the circumstancial effect is limited,
567 failing pairs resulting from a structural difference in the production of net rainfall.

568 Above all, the size effect was larger than these seasonal and physical distance effects. Runoff
569 discharge at the outlet results from integration of upstream variability in hydrological processes and
570 geography, but larger catchments also benefit from a wider spectrum of hydroclimate signals.
571 Consequently, discharge at the outlet represents more the mean of several hydroclimates and may

be more robust for transposition (both geomorphology-based and specific-discharge). Theoretically, the larger the donor catchment, the more distant the target catchment can be, as observed from the integrative metrics. Small→large transposition provides better results at short distances but decreases strongly at longer distances. In contrast, large→small transposition provides worse results at short distances, but with a less steep decrease with increasing distance.

5. Conclusion

This study, conducted in a nivo-pluvial context, identified critical functioning points of geomorphology-based inversion-transposition. Seasonality was identified as a major component of the effectiveness of transposition in Québec, Canada, highlighting variability in dominant flow paths in the resulting transposed net rainfall between pairs of catchments. Several pairs always experienced functioning or failing transposition, regardless of the metric or season, revealing structural differences between catchments. In addition, the Ghosh distance explained decreases in values of all metrics, with heterogeneities according to season, adding a circumstancial component to the previous structural one. Overall, either direction of geomorphology-based transposition (small→large or large→small) yielded better results than specific-discharge transposition, with the best results from small→large catchments. This confirms, like similar studies in two other hydrological regimes, the flexibility and realism of the geomorphology-based transposition approach to PUB.

590 **References**

591 Aouissi, J., Pouget, J.-C., Boudhraâ, H., Storer, G., Cudennec, C., 2013. Joint spatial, topological and
592 scaling analysis framework of river-network geomorphometry. Géomorphol., 19(1): 7-16.
593 https://doi.org/10.4000/geomorphologie.10082
594 Archfield, S.A., Vogel, R.M., 2010. Map correlation method: Selection of a reference streamgage to
595 estimate daily streamflow at ungaged catchments. Water Resour. Res., 46(10).
596 https://doi.org/10.1029/2009wr008481
597 Beven, K., Wood, E.F., 1993. Flow routing and the hydrological response of channel networks.
598 Channel Netw. Hydrol., Chichester, 99-128 p. https://doi.org/10.1080/02626667909491869
599 Blöschl, G., Grayson, R.B., Sivapalan, M., 1995. On the representative elementary area (REA) concept
600 and its utility for distributed rainfall-runoff modelling. Hydrol. Process., 9(3-4): 313-330.
601 https://doi.org/10.1002/hyp.3360090307
602 Blöschl, G., Sivapalan, M., 1995. Scale issues in hydrological modelling: A review. Hydrol. Process.,
603 9(3-4): 251-290. https://doi.org/10.1002/hyp.3360090305
604 Blöschl, G., Sivapalan, M., Wagener, T., Viglione, A., Savenije, H., 2013. Runoff Prediction in
605 Ungauged Basins: Synthesis across Processes, Places and Scales. Cambridge University Press,
606 Cambridge, 484 p. https://doi.org/DOI: 10.1017/CBO9781139235761
607 Boudhraâ, H., Cudennec, C., Andrieu, H., Slimani, M., 2018. Net rainfall estimation by the inversion of
608 a geomorphology-based transfer function and discharge deconvolution. Hydrol. Sci. J., 63(2):
609 285-301. https://doi.org/10.1080/02626667.2018.1425801
610 Boudhraâ, H., Cudennec, C., Slimani, M., Andrieu, H., 2006. Inversion of geomorphology-based unit
611 hydrograph model: Physical interpretation and first implementation. IAHS Publ., 303: 391-
612 399.
613 Boudhraâ, H., Cudennec, C., Slimani, M., Andrieu, H., 2009. Hydrograph transposition between basins
614 through a geomorphology-based deconvolution-reconvolution approach. IAHS Publ., 333: 76-
615 83.
616 Bull, L.J., Kirkby, M.J., 2002. Channel heads and channel extension. Hydrology and Geomorphology of
617 Semi-Arid Channels, Chichester, 263-287 p. https://doi.org/10.1007/s11069-010-9598-2
618 Chargui, S., Slimani, M., Cudennec, C., 2013. Statistical distribution of rainy events characteristics and
619 instantaneous hyetographs generation (Merguellil watershed in central Tunisia). Arab. J.
620 Geosci., 6(5): 1581-1590. https://doi.org/10.1007/s12517-011-0440-2
621 Criss, R.E., Winston, W.E., 2008. Do Nash values have value? Discussion and alternate proposals.
622 Hydrol. Process., 22(14): 2723-2725. https://doi.org/10.1002/hyp.7072
623 Cudennec, C., 2000. Description mathématique de l'organisation du réseau hydrographique et
624 modélisation hydrologique. Ph.D. thesis, Ecole Nationale Supérieure Agronomique de
625 Rennes, Rennes, France, 262 p.
626 Cudennec, C., 2007. On width function-based unit hydrographs deduced from separately random
627 self-similar river networks and rainfall variability: Discussion of “Coding random self-similar
628 river networks and calculating geometric distances: 1. General methodology” and “2.
629 Application to runoff simulations”. Hydrol. Sci. J., 52(1): 230-237.
630 https://doi.org/10.1623/hysj.52.1.230
631 Cudennec, C., Fouad, Y., Sumarjo Gatot, I., Duchesne, J., 2004. A geomorphological explanation of the
632 unit hydrograph concept. Hydrol. Process., 18(4): 603-621. https://doi.org/10.1002/hyp.1368
633 Cudennec, C., Gelfan, A., Ren, L., Slimani, M., 2016. Hydrometeorology and Hydroclimate. Adv.
634 Meteorol., 2016: 1-4. https://doi.org/10.1155/2016/1487890
635 Cudennec, C., Slimani, M., Goulven, P., 2005. Accounting for sparsely observed rainfall space—time
636 variability in a rainfall—runoff model of a semiarid Tunisian basin. Hydrol. Sci. J., 50(4): 617-
637 630. https://doi.org/10.1623/hysj.2005.50.4.617

de Lavenne, A., 2013. Modélisation hydrologique à base géomorphologique de bassins versants non jaugés par régionalisation et transposition d'hydrogramme. Ph.D. thesis, Agrocampus Ouest, Rennes, France, 226 p.

de Lavenne, A., Boudhraâ, H., Cudennec, C., 2015. Streamflow prediction in ungauged basins through geomorphology-based hydrograph transposition. Hydrol. Res., 46(2): 291. https://doi.org/10.2166/nh.2013.099

de Lavenne, A., Cudennec, C., 2014. Prediction of streamflow from the set of basins flowing into a coastal bay. PIAHS, 365: 55-60. https://doi.org/10.5194/piahs-365-55-2015

de Lavenne, A., Skøien, J.O., Cudennec, C., Curie, F., Moatar, F., 2016. Transferring measured discharge time series: Large-scale comparison of Top-kriging to geomorphology-based inverse modeling. Water Resour. Res., 52(7): 5555-5576. https://doi.org/10.1002/2016wr018716

Dunne, T., Black, R.D., 1971. Runoff Processes during Snowmelt. Water Resour. Res., 7(5): 1160-1172. https://doi.org/10.1029/WR007i005p01160

Fan, Y., Bras, R.L., 1995. On the concept of a representative elementary area in catchment runoff. Hydrol. Process., 9(7): 821-832. https://doi.org/10.1002/hyp.3360090708

Feki, H., Slimani, M., Cudennec, C., 2012. Incorporating elevation in rainfall interpolation in Tunisia using geostatistical methods. Hydrol. Sci. J., 57(7): 1294-1314. https://doi.org/10.1080/02626667.2012.710334

Formetta, G., Mantilla, R., Franceschi, S., Antonello, A., Rigon, R., 2011. The JGrass-NewAge system for forecasting and managing the hydrological budgets at the basin scale: models of flow generation and propagation/routing. Geoscientific Model Dev., 4(4): 943-955. https://doi.org/10.5194/gmd-4-943-2011

Franchini, M., O'Connell, P.E., 1996. An analysis of the dynamic component of the geomorphologic instantaneous unit hydrograph. J. Hydrol., 175(1-4): 407-428. https://doi.org/10.1016/S0022-1694(96)80018-7

Ghosh, B., 1951. Random distances within a rectangle and between two rectangles. Calcutta Math. Soc., 43(1): 17-24.

Gianfagna, C.C., Johnson, C.E., Chandler, D.G., Hofmann, C., 2015. Watershed area ratio accurately predicts daily streamflow in nested catchments in the Catskills, New York. J. Hydrol.: Reg. Stud., 4: 583-594. https://doi.org/10.1016/j.ejrh.2015.09.002

Grimaldi, S., Petroselli, A., Nardi, F., 2012. A parsimonious geomorphological unit hydrograph for rainfall–runoff modelling in small ungauged basins. Hydrol. Sci. J., 57(1): 73-83. https://doi.org/10.1080/02626667.2011.636045

Gupta, V.K., Mesa, O.J., 1988. Runoff generation and hydrologic response via channel network geomorphology—Recent progress and open problems. J. Hydrol., 102(1-4): 3-28. https://doi.org/10.1016/0022-1694(88)90089-3

Guttman, L.A., 1950. The basis for scalogram analysis. Measurement and prediction, 4: 60-90.

Hrachowitz, M., Savenije, H., Bogaard, T.A., Tetzlaff, D., Soulsby, C., 2013a. What can flux tracking teach us about water age distribution patterns and their temporal dynamics? Hydrol. Earth Syst. Sci., 17(2): 533-564. https://doi.org/10.5194/hess-17-533-2013

Hrachowitz, M., Savenije, H.H.G., Blöschl, G., McDonnell, J.J., Sivapalan, M., Pomeroy, J.W., Arheimer, B., Blume, T., Clark, M.P., Ehret, U., Fenicia, F., Freer, J.E., Gelfan, A., Gupta, H.V., Hughes, D.A., Hut, R.W., Montanari, A., Pande, S., Tetzlaff, D., Troch, P.A., Uhlenbrook, S., Wagener, T., Winsemius, H.C., Woods, R.A., Zehe, E., Cudennec, C., 2013b. A decade of Predictions in Ungauged Basins (PUB)—a review. Hydrol. Sci. J., 58(6): 1198-1255. https://doi.org/10.1080/02626667.2013.803183

John, J.A., Draper, N.R., 1980. An Alternative Family of Transformations. Journal of the Royal Statistical Society. Series C (Applied Statistics), 29(2): 190-197. https://doi.org/10.2307/2986305

Kane, D.L., Stein, J., 1983. Water movement into seasonally frozen soils. Water Resour. Res., 19(6): 1547-1557. https://doi.org/10.1029/WR019i006p01547

690 Karlsen, R.H., Seibert, J., Grabs, T., Laudon, H., Blomkvist, P., Bishop, K., 2016. The assumption of
691 uniform specific discharge: unsafe at any time? Hydrol. Process., 30(21): 3978-3988.
692 https://doi.org/10.1002/hyp.10877
693 Kingumbi, A., Bargaoui, Z., Hubert, P., 2005. Investigation of the rainfall variability in central Tunisia.
694 Hydrol. Sci. J., 50(3). https://doi.org/10.1623/hysj.50.3.493.65027
695 Kirkby, M., 1976. Tests of the random network model, and its application to basin hydrology. Earth
696 Surf. Process., 1(3): 197-212. https://doi.org/10.1002/esp.3290010302
697 Lacombe, G., Cappelaere, B., Leduc, C., 2008. Hydrological impact of water and soil conservation
698 works in the Merguellil catchment of central Tunisia. J. Hydrol., 359(3-4): 210-224.
699 https://doi.org/10.1016/j.jhydrol.2008.07.001
700 McMillan, H., Westerberg, I., Branger, F., 2017. Five guidelines for selecting hydrological signatures.
701 Hydrol. Process., 31(26): 4757-4761. https://doi.org/10.1002/hyp.11300
702 MDDELCC, DEB, 2018. Cadre écologique de référence du Québec (CERQ) [Données numériques
703 vectorielles]. In: Québec, G.d. (Ed.). Gouvernement du Québec.
704 Menke, W., 1989. Geophysical data analysis: Discrete inverse theory. Academic press, INC. Harcourt
705 Brace Jovanovich Ed., 45. https://doi.org/10.1016/C2011-0-69765-0
706 Merheb, M., Moussa, R., Abdallah, C., Colin, F., Perrin, C., Baghdadi, N., 2016. Hydrological response
707 characteristics of Mediterranean catchments at different time scales: a meta-analysis.
708 Hydrol. Sci. J., 61(14): 2520-2539. https://doi.org/10.1080/02626667.2016.1140174
709 Muleta, M.K., 2012. A Formal, Bayesian Approach for Uncertainty Analysis of a Watershed Model. In:
710 Engineers, A.S.o.C. (Ed.), World Environ. Water Resour. Congr. 2012. Proceedings.
711 https://doi.org/10.1061/9780784412312.375
712 Nash, J.E., Sutcliffe, J.V., 1970. River flow forecasting through conceptual models part I — A
713 discussion of principles. J. Hydrol., 10(3): 282-290. https://doi.org/10.1016/0022-
714 1694(70)90255-6
715 Nasri, S., Albergel, J., Cudennec, C., Berndtsson, R., 2004a. Hydrological processes in macrocatchment
716 water harvesting in the arid region of Tunisia: the traditional system of tabias. Hydrol. Sci. J.,
717 49(2). https://doi.org/10.1623/hysj.49.2.261.34838
718 Nasri, S., Cudennec, C., Albergel, J., Berndtsson, R., 2004b. Use of a geomorphological transfer
719 function to model design floods in small hillside catchments in semiarid Tunisia. J. Hydrol.,
720 287(1): 197-213. https://doi.org/10.1016/j.jhydrol.2003.10.001
721 Ogilvie, A., Belaud, G., Massuel, S., Mulligan, M., Le Goulven, P., Calvez, R., 2018. Surface water
722 monitoring in small water bodies: potential and limits of multi-sensor Landsat time series.
723 Hydrol. Earth Syst. Sci., 2018: 1-35. https://doi.org/10.5194/hess-2018-19
724 Ogilvie, A., Le Goulven, P., Leduc, C., Calvez, R., Mulligan, M., 2016. Hydrological response of a semi-
725 arid catchment to rainfall events and water and soil conservation works (Merguellil
726 catchment, central Tunisia). Hydrol. Sci. J., 61(2): 441-453.
727 https://doi.org/10.1080/02626667.2014.934249
728 Oudin, L., Andréassian, V., Mathevet, T., Perrin, C., Michel, C., 2006. Dynamic averaging of rainfall-
729 runoff model simulations from complementary model parameterizations. Water Resour.
730 Res., 42(7). https://doi.org/10.1029/2005wr004636
731 Parajka, J., Viglione, A., Rogger, M., Salinas, J.L., Sivapalan, M., Blöschl, G., 2013. Comparative
732 assessment of predictions in ungauged basins - Part 1: Runoff-hydrograph studies. Hydrol.
733 Earth Syst. Sci., 17(5): 1783-1795. https://doi.org/10.5194/hess-17-1783-2013
734 Pomeroy, J., Spence, C., Whitfield, P., 2013. Putting prediction in ungauged basins into practice. Can.
735 Water Resour. Assoc., Alberta, 375 p.
736 R Development Core Team, 2017. R: A Language and Environment for Statistical Computing.
737 Rigon, R., Bancheri, M., Formetta, G., de Lavenne, A., 2016. The geomorphological unit hydrograph
738 from a historical-critical perspective. Earth Surf. Process. Landf., 41(1): 27-37.
739 https://doi.org/10.1002/esp.3855

Robinson, J.S., Sivapalan, M., 1996. Instantaneous response functions of overland flow and subsurface stormflow for catchment models. Hydrol. Process., 10(6): 845-862. https://doi.org/10.1002/(SICI)1099-1085(199606)10:6<845::AID-HYP375>3.0.CO;2-7

Robinson, J.S., Sivapalan, M., Snell, J.D., 1995. On the relative roles of hillslope processes, channel routing, and network geomorphology in the hydrologic response of natural catchments. Water Resour. Res., 31(12): 3089-3101. https://doi.org/10.1029/95wr01948

Rodríguez-Iturbe, I., Valdés, J.B., 1979. The geomorphologic structure of hydrologic response. Water Resour. Res., 15(6): 1409-1420. https://doi.org/10.1029/WR015i006p01409

Seiller, G., Roy, R., Anctil, F., 2017. Influence of three common calibration metrics on the diagnosis of climate change impacts on water resources. J. Hydrol., 547: 280-295. https://doi.org/10.1016/j.jhydrol.2017.02.004

Sivakumar, B., 2007. Dominant processes concept, model simplification and classification framework in catchment hydrology. Stoch. Environ. Res. Risk Assess., 22(6): 737-748. https://doi.org/10.1007/s00477-007-0183-5

Sivapalan, M., Takeuchi, K., Franks, S.W., Gupta, V.K., Karambiri, H., Lakshmi, V., Liang, X., McDonnell, J.J., Mendiondo, E.M., O'Connell, P.E., Oki, T., Pomeroy, J.W., Schertzer, D., Uhlenbrook, S., Zehe, E., 2003. IAHS decade on Predictions in Ungauged Basins (PUB), 2003-2012: Shaping an exciting future for the hydrological sciences. Hydrol. Sci. J., 48(6): 857-880. https://doi.org/10.1623/hysj.48.6.857.51421

Skøien, J.O., Blöschl, G., Laaha, G., Pebesma, E., Parajka, J., Viglione, A., 2014. rtop: An R package for interpolation of data with a variable spatial support, with an example from river networks. Comput. & Geosci., 67: 180-190. https://doi.org/10.1016/j.cageo.2014.02.009

Skøien, J.O., Merz, R., Blöschl, G., 2006. Top-kriging - geostatistics on stream networks. Hydrol. Earth Syst. Sci., 10(2): 277-287. https://doi.org/10.5194/hess-10-277-2006

Sneath, P.H.A., 1957. The application of computers to taxonomy. Microbiology, 17(1): 201-226.

Snell, J.D., Sivapalan, M., 1994. On geomorphological dispersion in natural catchments and the geomorphological unit hydrograph. Water Resour. Res., 30(7): 2311-2323. https://doi.org/10.1029/94wr00537

Spence, C., Whitfield, P.H., Pomeroy, J.W., Pietroniro, A., Burn, D.H., Peters, D.L., St-Hilaire, A., 2013. A review of the Prediction in Ungauged Basins (PUB) decade in Canada. Can. Water Resour. J., 38(4): 253-262. https://doi.org/10.1080/07011784.2013.843867

Surkan, A.J., 1969. Synthetic hydrographs: effects of network geometry. Water Resour. Res., 5(1): 112-128. https://doi.org/10.1029/WR005i001p00112

Tarantola, A., 1987. Inverse Problem Theory: Methods for Data Fitting and Model Parameter Estimation. Elsevier, Amsterdam, 644 p.

Tarantola, A., Valette, B., 1982. Inverse problems= quest for information. J. Geophys., 50(3): 150-170.

Tremblay, Y., Rousseau, A.N., Plamondon, A.P., Lévesque, D., Jutras, S., 2008. Rainfall peak flow response to clearcutting 50% of three small watersheds in a boreal forest, Montmorency Forest, Québec. J. Hydrol., 352(1-2): 67-76. https://doi.org/10.1016/j.jhydrol.2007.12.028

Wang, C., Gupta, V.K., Waymire, E., 1981. A geomorphologic synthesis of nonlinearity in surface runoff. Water Resour. Res., 17(3): 545-554. https://doi.org/10.1029/WR017i003p00545

Wood, E.F., Sivapalan, M., Beven, K., Band, L., 1988. Effects of spatial variability and scale with implications to hydrologic modeling. J. Hydrol., 102(1-4): 29-47. https://doi.org/10.1016/0022-1694(88)90090-x

Woods, R., Sivapalan, M., 1999. A synthesis of space-time variability in storm response: Rainfall, runoff generation, and routing. Water Resour. Res., 35(8): 2469-2485. https://doi.org/10.1029/1999WR900014